PROCEEDINGS OF SCIENCE

Search for charged Higgs bosons with the $H^{\pm} \to \tau^{\pm}\nu_{\tau}$ decay channel

Jan Eysermans*, **María Isabel Pedraza Morales for the CMS Collaboration**
Benemérita Universidad Autónoma de Puebla, Mexico
E-mail: jan.eysermans@cern.ch

A search for charged Higgs bosons decaying into a tau lepton and a neutrino is presented in the hadronic and leptonic final states. The search is based on the 13 TeV dataset with 35.9 fb^{-1} of integrated luminosity collected with the CMS experiment in 2016. Results are presented for charged Higgs boson mass hypotheses ranging from 80 GeV to 3 TeV, where the intermediate mass range around the top quark mass is included. 95% CL upper limits are set on the charged Higgs boson production cross section. The model independent result is interpreted in the MSSM m_h^{mod-} benchmark scenario.

Prospects for Charged Higgs Discovery at Colliders - CHARGED2018
25-28 September 2018
Uppsala, Sweden

*Speaker.

PoS(CHARGED2018)007

1. Introduction

In the Standard Model (SM), the electroweak gauge bosons W and Z vector bosons acquire mass through the Higgs mechanism, which is based on the spontaneous symmetry breaking of a Higgs doublet ϕ in a scalar potential $V(\phi)$. Extensions of the SM in the Higgs sector introduce one or more doublets resulting in a richer bosonic particle spectrum able to explain phenomena for which the SM fails. In particular, the Two Higgs Doublet Model (2HDM), two doublets ϕ_1 and ϕ_2 are introduced with a modified potential $V(\phi_1, \phi_2)$, resulting in 5 Higgs bosons in the spectrum after the electroweak symmetry breaking [1]:

- CP even, neutral: h (125 GeV), H;
- CP odd, neutral pseudoscalar A;
- charged $H^{\pm}$.

Observation of one of these bosons (with the exception of the SM Higgs) leads unequivocally to physics beyond the SM. So far no additional boson has been observed and direct searches for such bosons put constraints in the parameter space of the 2HDM [2].

This work focuses on charged Higgs bosons, for which the mass parameter is unconstrained and can have a value in the range from GeV to the TeV scale. The production depends on its mass: for charged Higgs bosons below the top quark mass, the dominant production mode is from decays of the top quarks (mainly from $t\bar{t}$ production). For charged Higgs bosons above the top quark mass, associated production $tH^{+}(b)$ is dominant in the 5FS(4FS). Charged Higgs boson mases around the top quark mass involve interference effects as well as top width effects and the full process $pp \to \mathrm{H}^{\pm}\mathrm{W}^{\pm}bb$ must be taken into account [3].

For what concerns the charged Higgs boson decay, several Yukawa coupling schemes are possible which are defined based on the coupling combinatorics of particle generation and the doublet fields. In particular, in the type-II the up-type quarks couple to ϕ_2 whereas the down-type quarks and charged leptons couple to ϕ_1, which give rise to an enhanced coupling to the third generation particles (t, b, τ). As a result, the tb and $\tau\nu$ final states are interesting for direct charged Higgs searches and put constraints on the 2HDM parameter space in type-II.

This work covers the $\mathrm{H}^{\pm} \to \tau^{\pm}\nu_{\tau}$ decay mode in both hadronic and leptonic final states [4]. A broad mass range from 80 GeV to 3 TeV is probed including the challenging intermediate mass range around the top quark mass. The results are based on the 13 TeV dataset with 35.9 fb^{-1} of integrated luminosity collected with the CMS experiment [5] in 2016.

2. Hadronic final state

The hadronic final state requires the presence of a hadronically decaying τ-lepton (τ_h) in association with large $\mathrm{E}_{\mathrm{T}}^{\mathrm{miss}}$ from the neutrinos (see Figure 1). Additional jets are present from the hadronic top quark decays. The presence of any lepton (electron, muon) is vetoed. Because all neutrinos originate from the charged Higgs decay, the transverse mass reconstruction is possible using $\tau_h + \mathrm{E}_{\mathrm{T}}^{\mathrm{miss}}$ system:

$$m_T = \sqrt{2p_T(\tau_h)\mathrm{E}_{\mathrm{T}}^{\mathrm{miss}}(1 - \cos\Delta\phi(\vec{p}_{\mathrm{T}}(\tau_h), \vec{p}_{\mathrm{T}}^{\mathrm{miss}}))}.$$

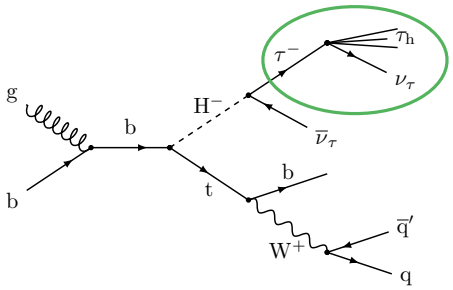

Figure 1: Feynman diagram of the hadronic final state.

2.1 Event selection and categorization

Events are selected using an online trigger composed of a τ_h and $\mathrm{E_T^{miss}}$ leg with respective p_T thresholds of 50 and 90 GeV, with an additional selection on the τ_h leading track p_T of 30 GeV. Further offline selection criteria are applied which are optimized to enhance signal sensitivity:

- hadronically decaying tau lepton, 1-prong only;
- $\mathrm{E_T^{miss}} > 90$ GeV;
- at least 3 jets, one b-tagged jet;
- veto on electrons or muons.

An additional angular cut to suppress jet $\to$ fake τ_h backgrounds (mainly from QCD multijets) is applied, defined as follows:

$$R_{\mathrm{bb}}^{\mathrm{min}} = \min\left\{\sqrt{\left(180^{\circ} - \Delta\phi(\tau_h, \vec{p}_{\mathrm{T}}^{\mathrm{miss}})\right)^2 + \left(\Delta\phi(\mathrm{jet}_n, \vec{p}_{\mathrm{T}}^{\mathrm{miss}})\right)^2}\right\} > 40^{\circ}.$$

This formula is justified by considering that the majority of QCD multijet events have a back-to-back di-jet pair, where one of the jets is mis-identified as a τ jet. Hence the $\mathrm{E_T^{miss}}$ is overestimated in the mis-identified τ direction which simultaneously minimizes $\Delta\phi(\tau_h, \vec{p}_{\mathrm{T}}^{\mathrm{miss}})$ and maximizes $\Delta\phi(\mathrm{jet}_n, \vec{p}_{\mathrm{T}}^{\mathrm{miss}})$, where n runs over the reconstructed jets. An optimal working point of 40° has been chosen across entire mass range (see Fig. 2 (left)).

In order to further enhance the signal sensitivity, the event phase space is divided in two categories by exploiting the difference in polarization states of the τ_h originating either from $\mathrm{H}^{\pm}$ decays (scalar, left-handed τ_h) or from $\mathrm{W}^{\pm}$ decays. (vector, right-handed τ_h). Because longitudinal polarization states tend to have a higher leading track p_T, the variable R_{τ} defined as

$$R_{\tau} = \frac{p_T(\text{leading track})}{p_T(\tau_h)},$$

is sensitive to the τ_h polarization state, as can be seen from Fig. 2 (right). Indeed, for low values of R_{τ} the backgrounds are dominant whereas at high values of R_{τ} the distribution is more pure in signal. Events are categorized based on $R_{\tau} > 0.75$ and $R_{\tau} < 0.75$ which is also optimized across entire mass range.

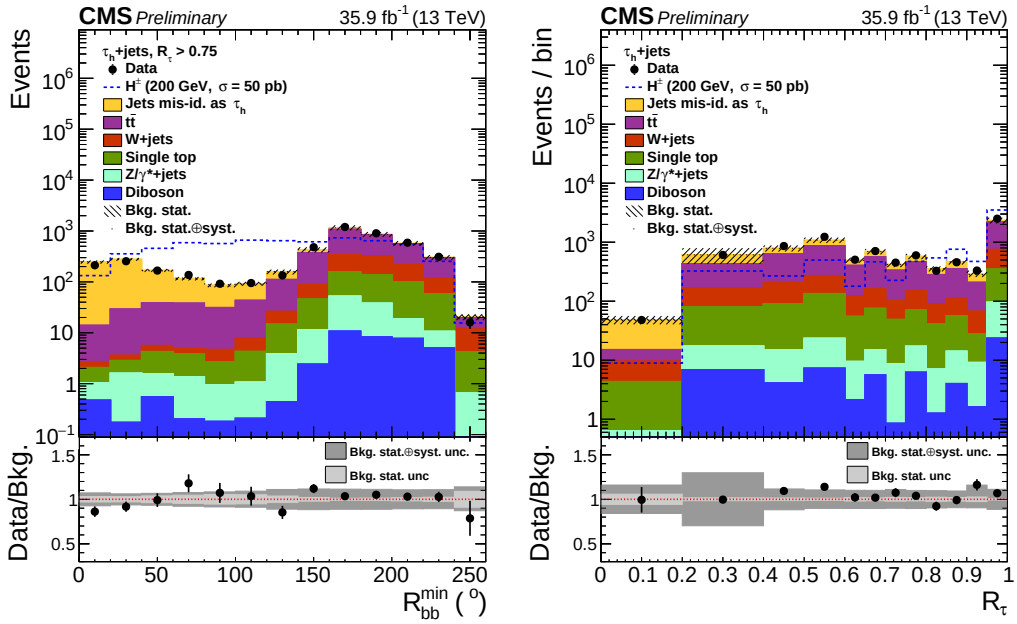

Figure 2: Left: distribution of the R_{bb}^{min} variable where it can be seen that the jet $\to$ fake τ_h background piles up at low values of R_{bb}^{min}. Right: R_{τ} distribution which separates the signal (high R_{τ}) and background (low R_{τ}) τ_h polarization states [4].

3. Leptonic final states

The search for a charged Higgs boson in the $H^{\pm} \to \tau^{\pm}\nu_{\tau}$ (single) leptonic final state is conducted in two categories based on whether a hadronically decaying tau lepton can be resolved or not: $\ell + \tau_h$ and $\ell +$ no τ_h respectively (see Fig. 3 for example Feynman diagrams). This division is motivated by the different background natures and different signal sensitivities in those categories. Indeed, in the $\ell + \tau_h$ two leptons (τ_h and ℓ) are present with as major background dileptonic $t\bar{t}$ events whereas for the $\ell +$ no τ_h category only the semileptonic $t\bar{t}$ background is abundant. Apart from the lepton and optionally a τ_h, signal-like events also contain large E_T^{miss} due to the neutrinos involved and jets, for which at least one is a b-jet originating from top decay.

Signal extraction is also based on the transverse mass distribution reconstructed from the ℓ + E_T^{miss} system:

$$m_T = \sqrt{2p_T(\ell)E_T^{miss}(1-\cos\Delta\phi(\vec{p}_T(\ell),\vec{p}_T^{miss}))}.$$

However, due to the presence of additional neutrinos from the τ decay and neutrino from the semileptonic top decay especially in the $\ell + \tau_h$ category, the m_T distribution is more smeared and does not exhibit a sharp peak at the endpoint mass.

Furthermore, the event phase space with high jet multiplicities is found to be more sensitive in the $H^{\pm} \to tb$ leptonic analysis and therefore the $H^{\pm} \to \tau^{\pm}\nu_{\tau}$ leptonic final state is limited with a jet multiplicity up to 3.

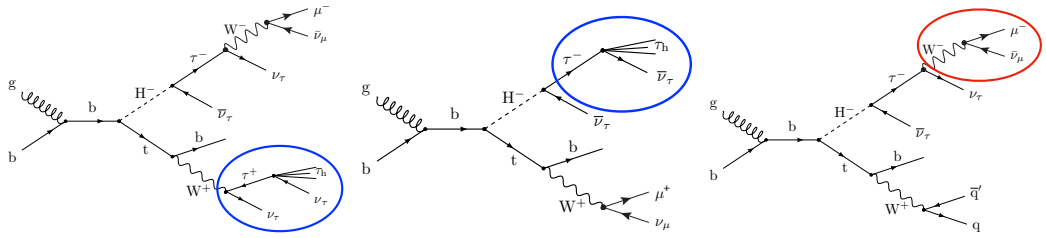

Figure 3: Feynman diagrams for the $\ell + \tau_h$ category (left, center) and the $\ell +$ no τ_h category (right) [4].

3.1 Event selection

Events are selected using online lepton triggers, separately for both electron and muon final states. Several triggers are combined to gain efficiency at high lepton p_T. Opposed to the hadronic final state, the leptonic final states make use of a loose (offline) event selection with a large categorization to enhance signal sensitivity and to constrain the backgrounds and their uncertainties. For the $\ell + \tau_h$ final state, the event selection is given by:

- lepton + trigger + hadronic τ;
- $E_T^{miss} > 70$ GeV;
- one, two or three jets, at least one b-tagged jet;
- veto on additional loose leptons;
- $\Delta\phi(E_T^{miss}, \ell) > 0.5$ (*non-prompt leptons*).

A similar event selection is applied to the $\ell +$ no τ_h final state:

- lepton + trigger + veto hadronic τ;
- $E_T^{miss} > 100$ GeV;
- one, two or three jets, at least one b-tagged jet;
- veto on additional loose leptons;
- $\Delta\phi(E_T^{miss}, \ell) > 0.5$ (*non-prompt leptons*);
- $\Delta\phi(E_T^{miss}, \text{leading jet}) > 0.5$ (*fake leptons*);
- $\min(\Delta\phi(\ell, \text{jet})) < \pi - 0.5$ (*jet mismeasurements*).

The high E_T^{miss} thresholds and angular cuts suppress fake leptons and taus to a negligible amount. Fake leptons originate from QCD multijet events or from muonic b-hadron decays (non-prompt leptons).

3.2 Categorization

Based on the loose event selection described above, a categorization is performed to enhance signal sensitivity, to constrain the backgrounds (mainly $t\bar{t}$) and the associated uncertainties. The categorization is performed in three dimensions: jet multiplicity, b-jet multiplicity and E_T^{miss}, for both electron and muon final states.

The jet related categorization mainly exploits the constrains of the dominant systematics. Furthermore the signal sensitivity changes for different categories and for different charged Higgs

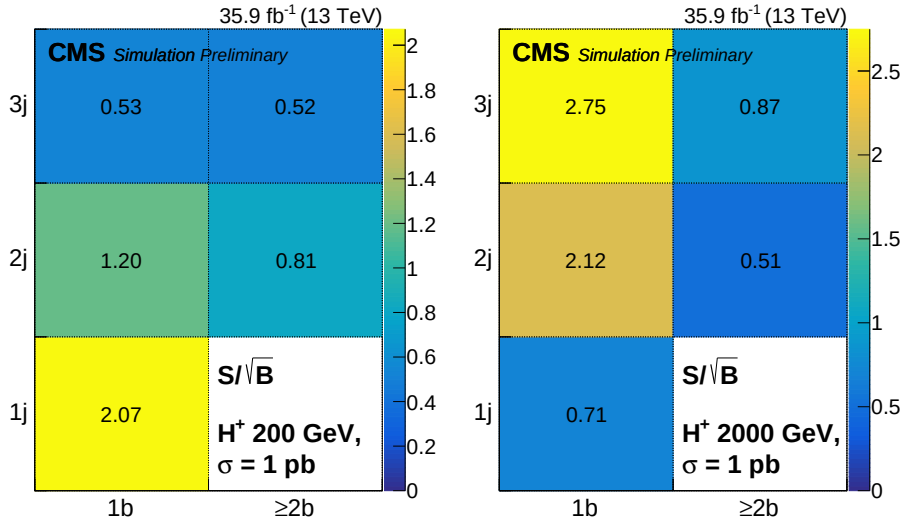

Figure 4: Significance $S/\sqrt{B}$ for each of the jet categories for a charged Higgs mass of 200 GeV (left) and 2 TeV (right). $S(B)$ represents the total signal(background) yield in that category; the signal is normalized to 1 pb [4].

masses. In particular for higher charged Higgs masses, the sensitivity is pushed towards higher jet multiplicities as can be seen from Fig. 4 where the significance is given in each category for a low and high mass hypothesis. 3 categories are used for the $\ell + \tau_h$ category: 1j/1b, 2-3j/1b and 2-3j/2-3b. For the $\ell +$ no τ_h, 4 categories are used: 2j/1b, 2j/2b, 3j/1b and 3j/2-3b.

Another categorization in bins of E_T^{miss} is performed to enhance signal sensitivity. Low values of E_T^{miss} are background abundant whereas higher E_T^{miss} regions are more pure in signal. 3 categories are used for the $\ell + \tau_h$ category: $70 < E_T^{miss} < 100$ GeV, $100 < E_T^{miss} < 150$ and $E_T^{miss} > 150$ GeV. For the $\ell +$ no τ_h, only two categories are used due to the higher E_T^{miss} threshold: $100 < E_T^{miss} < 150$ and $E_T^{miss} > 150$ GeV.

4. Background estimation

The major backgrounds are jet $\to$ fake τ_h (hadronic final state only), $t\bar{t}$ and W+jets. Minor backgrounds such as single top, DY+jets and diboson are also considered in the analysis. All backgrounds are estimated from simulation, except the jet $\to$ fake τ_h which is estimated using a data-driven technique (fake rate).

The data-driven method in the hadronic final state consists of deriving transfer factors in a loose region (pure in fake τ_h) between the nominal and inverted τ_h isolation. The transfer factors are derived in bins of τ_h p_T and η to minimize correlations and mitigation of detector inefficiencies. To estimate the jet $\to$ fake τ_h in signal region, the transfer factors are applied in the application region.

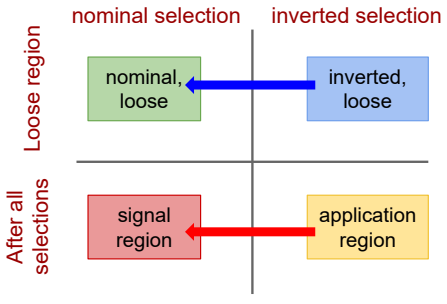

5. Intermediate mass range

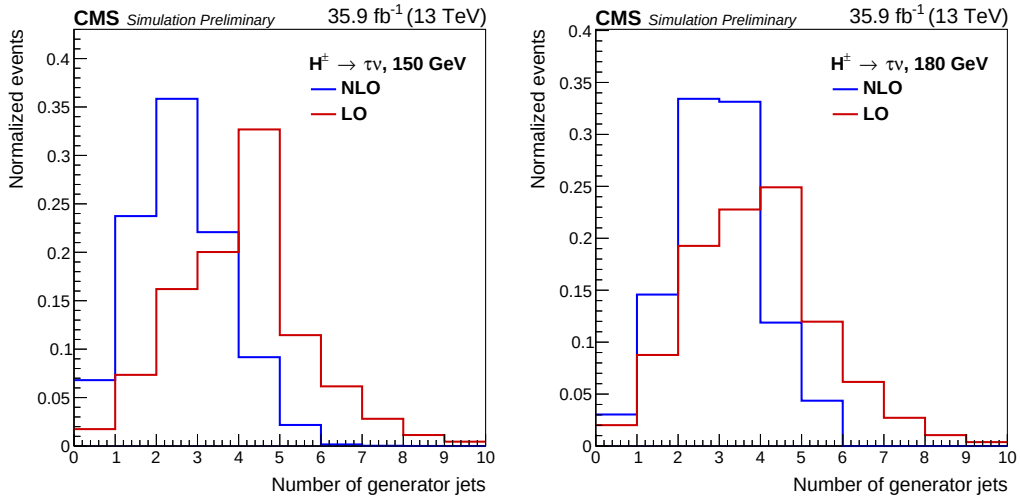

Figure 5: Normalized generator jet multiplicity distributions for both LO (red) and NLO (blue), for charged Higgs masses of 150 GeV (light production mode, left) and 180 GeV (heavy production mode, right) [4].

For charged Higgs masses around the top quark mass, the interference of the heavy and light charged Higgs production modes must be taken into account as well as top-width effects [3]. Several resonances contribute to the total cross section of the intermediate charged Higgs masses, where also resonances with neutral scalars (H, A) must be taken into account. Due to the interplay of the neutral scalars, the charged Higgs production mode becomes model dependent and therefore they are omitted to avoid such model dependencies. Currently, from theory point of view it is difficult to calculate the interference effects up to NLO accuracy level, therefore only the leading order results are available. Because the light and heavy mass samples are generated at NLO, a re-scaling procedure on the intermediate LO samples has been applied.

Differences between LO and NLO are studied based on LO samples in overlap with the light NLO (140–160 GeV) and heavy NLO (180–220 GeV) samples. It has been found their m_T shapes are similar, though deviations in acceptance from jet multiplicity and production mode (light vs. heavy) have been observed. This is shown in Fig. 5 where the normalized generator jet multiplicity distributions are shown for both LO and NLO, for charged Higgs masses of 150 GeV (light production mode) and 180 GeV (heavy production mode). To cope with these acceptance differences, NLO/LO scale factors are derived using the overlapping samples:

- derived for both light (140–160 GeV) and heavy mass (180–220 GeV) regime;
- derived in each category of the final states.

The scale factors are applied to the intermediate mass samples for 165 GeV (light scale factors) and 170/175 GeV (heavy scale factors). Statistical uncertainties in the scale factors are taken into account as normalization uncertainties.

6. Results

A simultaneous fit based on the hadronic and leptonic m_T templates is performed by means of a binned maximum likelihood fit. In total 36 m_T templates are fitted: 2 hadronic templates, 18 templates from the $\ell + \tau_h$ category and 16 from the $\ell +$no τ_h category. Experimental and theoretical uncertainties are incorporated in the likelihood as profiled nuisance parameters. The most impacting nuisances are related to the τ_h identification and the modelling of $t\bar{t}$ especially in the leptonic final states.

No excess in data is observed after the fit which means the result is in agreement with the Standard Model prediction. 95% CL exclusion limits on charged Higgs cross section times branching fraction are set within the asymptotic approximation [6]. The results are shown in Fig. 6 (left), where the upper limit is shown from 80 GeV to 3 TeV charged Higgs mass hypotheses, including the intermediate mass range. The sensitivity ranges from ≈ 6 pb at low mass to ≈ 4.8 fb at high mass.

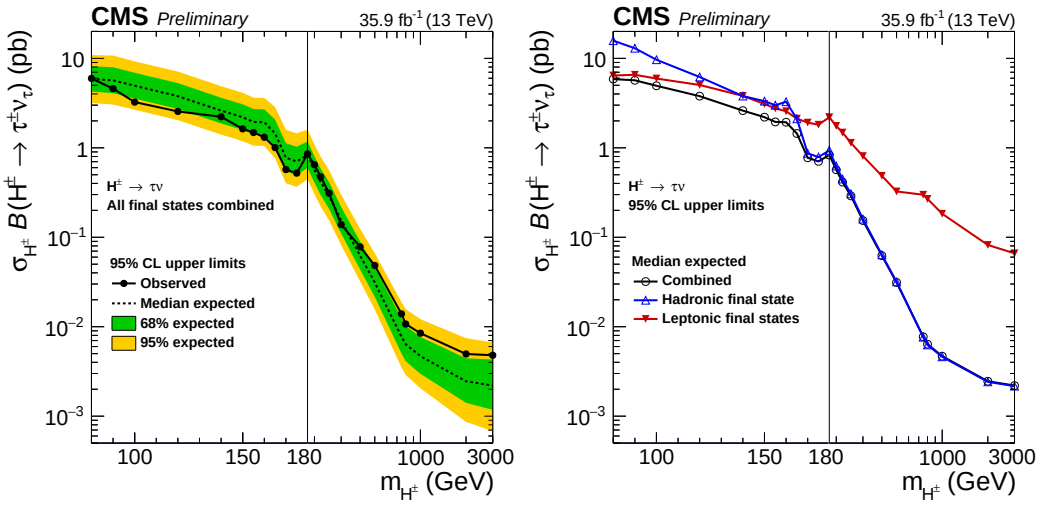

Figure 6: Left: 95% CL exclusion limits on charged Higgs cross section times branching fraction. Right: expected upper limit for the hadronic final state (blue), leptonic final states (red) and combined result (black)[4].

On Fig. 6 (right), the hadronic (blue) and leptonic (red) expected limits are shown separately and compared to the combined result (black). At low mass, the leptonic final state is dominant because it benefits from categorization and background constraints due to high statistics whereas the hadronic final state is constrained by E_T^{miss} and τ p_T trigger thresholds. On the other hand at high mass the hadronic final state is fully dominant due to the clear m_T shape and the limitation of jet multiplicity in the leptonic final state.

Model dependent interpretation. The model independent upper limits are interpreted in a Minimal Supersymmetric Standard Model (MSSM) benchmark scenario. In the MSSM, which is described in the type-II 2HDM, only two free parameters are present: the mass of the charged Higgs ($m_{H^{\pm}}$) and $\tan\beta = v_2/v_1$, where v_i is the vacuum expectation value of doublet i [7]. The other remaining parameters in the 2HDM are fixed which leads to several interpretative scenarios. Shown in Fig. 7 is the exclusion of the value of $\tan\beta$ as function of $m_{H^{\pm}}$ for the MSSM m_h^{mod-} scenario.

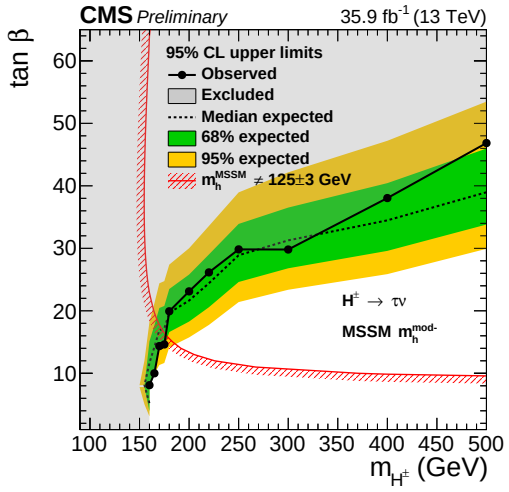

Figure 7: Model dependent exclusion of $\tan\beta$ as function of $m_{\mathrm{H}^{\pm}}$ for the MSSM $\mathrm{m}_{\mathrm{h}}^{\mathrm{mod-}}$ scenario [4].

7. Conclusions

In this work the CMS $\mathrm{H}^{\pm} \to \tau^{\pm}\nu_{\tau}$ result is presented based on the 13 TeV dataset with 35.9 fb^{-1} of integrated luminosity. Both hadronic and leptonic final states are considered over a broad mass range from 80 GeV to 3 TeV, with the inclusion of the intermediate mass regime. Results are in agreement with the Standard Model prediction and 95% CL exclusion limits are set on the charged Higgs production times branching fraction. The model independent result is interpreted in a MSSM benchmark scenario.

References

[1] G. C. Branco, P. M. Ferreira, L. Lavoura, M. N. Rebelo, M. Sher and J. P. Silva, "Theory and phenomenology of two-Higgs-doublet models," Phys. Rept. **516**, 1 (2012) doi:10.1016/j.physrep.2012.02.002 [arXiv:1106.0034 [hep-ph]].

[2] CMS Collaboration, "Search for a charged Higgs boson in pp collisions at $\sqrt{s} = 8$ TeV," JHEP **1511** (2015) 018 doi:10.1007/JHEP11(2015)018 [arXiv:1508.07774 [hep-ex]].

[3] C. Degrande, R. Frederix, V. Hirschi, M. Ubiali, M. Wiesemann and M. Zaro, "Accurate predictions for charged Higgs production: Closing the $m_{H^{\pm}} \sim m_t$ window," Phys. Lett. B **772** (2017) 87 doi:10.1016/j.physletb.2017.06.037 [arXiv:1607.05291 [hep-ph]].

[4] CMS Collaboration, "Search for charged Higgs bosons with the $\mathrm{H}^{\pm} \to \tau^{\pm}\nu_{\tau}$ decay channel in proton-proton collisions at $\sqrt{s} = 13$ TeV," http://cds.cern.ch/record/2640359.

[5] CMS Collaboration, "The CMS Experiment at the CERN LHC," JINST **3** (2008) S08004. doi:10.1088/1748-0221/3/08/S08004

[6] A. L. Read, "Presentation of search results: The CL(s) technique," J. Phys. G **28**, 2693 (2002). doi:10.1088/0954-3899/28/10/313

[7] M. Carena, S. Heinemeyer, O. Stål, C. E. M. Wagner and G. Weiglein, "MSSM Higgs Boson Searches at the LHC: Benchmark Scenarios after the Discovery of a Higgs-like Particle," Eur. Phys. J. C **73**, no. 9, 2552 (2013) doi:10.1140/epjc/s10052-013-2552-1 [arXiv:1302.7033 [hep-ph]].